J. Indian Chem. Soc.,
Vol. 97, No. 11a, November 2020, pp. 2224-2232

Sequestration of Pb(II), Ni(II) and Zn(II) biosorption onto brown seaweed *Sargassum wightii:* Isotherm and kinetic modeling

J. Vijayaraghavan*[a], D. Zunaithur Rahman[b] and J. Thivya[c]

[a]Department of Civil Engineering, University College of Engineering Ramanathapuram, Ramanathapuram-623 513, Tamil Nadu, India

[b]Department of Civil Engineering, Aalim Muhammed Salegh College of Engineering, Chennai-600 055, India

[c]Department of Civil Engineering, University College of Engineering Dindigul, Dindigul-624 622, Tamil Nadu, India

E-mail: drjvr1988@gmail.com

Manuscript received online 12 October 2020, revised and accepted 30 November 2020

This analysis is aimed at exploring the potential of brown seaweed *Sargassum wigtii* for the sequestration of lead, nickel, and zinc metal ions from aqueous solutions. The biosorption process was identified by FTIR and SEM analytics on the contact between positive metal ions and negatively-charged functional groups on *S. wightii*'s surface. Biosorption isotherms obtained at pH 5, 4, and 8 for Pb(II), Ni(II), and Zn(II) indicate that the seaweed provides a greater intake of Pb (86.37 mg/g), with Zn (70.16 mg/g) and Ni (56.74 mg/g). The above-mentioned pH mechanism significantly affected the biosorption capacity of brown algae. Such varying affinity was measured by atomic weight, the radius of metal ions, and the negative charges of electrons of the biosorbent for the three metal ions. The Toth model improved projected experimental isotherm results with strong correlation coefficients (R^2) from different isotherm models (Langmuir, Freundlich, Toth, and Sips). Kinetic tests found very strong metal removal efficiency by *S. wightii,* with 99% being completed in 90 min. Desorption tests with different elutant components (0.01 *M* NaOH, HCl, and EDTA) revealed that 0.01 *M* HCl could accomplish the highest desorption of all metal ions from metal-loaded *S. wightii*.

Keywords: Water treatment, biosorption, Pb, Ni and Zn, metal, *Sargassum wightii*, brown seaweed.

Introduction

Rising point sources of emissions and the need to clean up toxic runoff are recognized by the government and industry in recent years. The prevalence of heavy metals in wastewater, which are non-biodegradable, cause severe health concerns[1,2]. Many factories, in particular those involved in plating, coating, leather, and mining, produce vast volumes of wastewater with heavy metal concentrations. The risk of such heavy metals ensures that all contaminated products should be e treated before discharge[3]. The following constraints which include high cost, incomplete elimination, poor selectivity, high energy usage, and production of toxic slurries have already been established for the traditional processing methods or recovery of toxic wastewater pollutants through adsorption, exchange of ions, precipitation, electrosorption, and adding oxygen and reduction processes[4,5]. Therefore, new inexpensive and effective solutions are desperately required to replace current methods in treating wastewater contaminated with heavy metals[6,7].

Biosorption is an effective method for liquid treatment of heavy metals. The process consists of solid and liquid phases. The latter is drawn and attached to the sorbent by different paths due to the higher affinity of the sorbent for the sorbate. The cycle continues until an equilibrium between the quantity of firmly bonded sorbate species and its share is defined. Metal sorption through biosorbents is achieved by ion exchange and/or variations of such processes via complexation, synchronization and, chelation[8,9]. Various biosorbents, like inactive/dead microbes, fungi, algae, yeast, farm waste, and industrial waste have been widely used to extract heavy metal ions. The possibility of utilizing dead or inactive algae to function as possible heavy metal biosorbents was exten-

sively explored in recent years, as this method provides many advantages which include low operating cost, continuous biosorbent quality, good efficiency, and multi-cycle reusability[10–13]. Brown seaweed was researched extensively for heavy metal ions in recent years. However, biosorption work has concentrated less on red and green sea algae[14,15]. Hashim *et al.*[16] recorded a few biosorption experiments utilizing red algae (*Gracilaria salicornia*) that demonstrated the lowest uptake of 0.16 mmol/g among various species of marine algae tested for Cd biosorption. Vijayaraghavan *et al.*[17] described red and brown algae of *Gracilaria* and *Geledium* species and *Sargassum wightii* and *illcifolium* for removal of cobalt and nickel ions with high efficiency. The key cause behind the poor biosorption of red algae is the composition of the cell wall. The red algae's cell wall is primarily made up of carrageen and agar (as opposed to brown seaweed alginates). However, the mediocre ability of biosorption was focused on a few species of brown algae and further work is required to explain the ability of other forms of brown algae[18,19].

This work focuses on the use of fresh brown alga *Sargassum wightii* for the biosorption of Pb(II), Ni(II), and Zn(II) *Sargassum* is one of the biggest and fast-growing tropical brown algae. While the algae have industrial uses, *Sargassum* organisms are highly destructive in certain areas of the world's environment due to their very high growth rate, plastic morphology, and exceptionally efficient vegetative regeneration. Therefore, an additional application of *S. wightii* is attractive and good[20]. The current work also provides insights into the process of binding heavy metal ions for removal by *S. wightii* and key parameters that influence their biosorption are defined.

Materials and methods

Collection of seaweed and preparation of the metal solution:

S. wightii was taken from the island beaches of Kurusadai, Mandapam, Tamilnadu, India (9°14′N 79°12′E). The algal biomass was washed in deionized water and dried in sunlight for 10 days. The algae were ground to an average particle size of 150–175 microns size and, then pulverized using a household mixer (1HP Micro active, India) and incurred for 6 h at 105°C. Pb(II), Ni(II), and Zn(II) stock solutions (1000 mg/L) were developed with $PbSO_4$, $NiSO_4.6H_2O$, and $ZnSO_4.7H_2O$. The metal solutions were diluted with DI water to obtain the required concentrations during the test. Analytical grade chemicals were obtained from Merck (India).

Procedure for the experimentation in metal biosorption:

Experiments were carried out with 250 mL Erlenmeyer bottles in a rotary shaker at room temperature. 0.2 g of seaweed was used in each flask in the correct concentration ranges for 100 ml for each of the three metal ions Pb(II), Ni(II), and Zn(II). The flasks were agitated in a 150 rpm rotary shaker (PS Instruments, India), for 4 h. Originally, 0.1 *M* HCl or NaOH was (added and controlled with a metal pH solution). The beaker's contents were centrifuged for 3 min at 4000 rpm during the biosorption treatment and the suspension was filtered through a Whatman filter sheet. The supernatant was examined using Atomic Absorption Spectroscopy (AAS Vario 6, Analytik Jena, Germany) to assess metal concentration. A pH-edge experiment is generally conducted at a fixed initial metal concentration of 100 mg/L in different pH conditions (pH 2–9). Instead, isotherm studies with different initial concentrations of metals (10–125 mg/L) were performed with an ideal pH. Optimal pH and initial metal concentration of 10 mg/L were performed in kinetic experiments. 0.1 mL samples were taken from the mixture to produce the kinetic results after a fixed duration.

The quantity of metal biosorbed by *S. wightii* was determined using the following equation, dependent on the discrepancy between the volume of metal in *S. wightii* and the concentration of metal after sorption,

$$Q = V(C_o - C_e)/M \quad (1)$$

when Q is the sorbent capacity (mg/g), V is the sorbate volume (L), C_o, and C_e are the initial and equilibrium metal in the solution (mg/L), and M the weight of *S. wightii* (g). After the biosorption test, metal-loaded *S. wightii* was filtered and eventually exposed in an Erlenmeyer flask to many elutant solutions for desorption studies. 50 mL of elutant solution was used to obtain the required concentration. The material was agitated for 60 min at 150 rpm. After filtration, AAS was used to assess the metal content of the supernatant for desorption. Desorption efficiency was calculated by comparing the solution metal ions after desorption with the initially bonded metal ions with the biosorbent. Non-linear regression using Sigma Plot (V4.0, SPSS, USA) evaluated the isotherm and kinetic model parameters.

Characterization of S. wightii:

A Fourier IR spectrometer transform (Perkin-Elmer, Spectrum RX1) was used to evaluate the process of metal extraction by *S. wightii* and the presence of functional groups. The samples were provided KBr as pellets. The samples were cleaned, filled with a fine gold coat, and then examined with a scanning electron microscope (JEOL JSM 6360, Japan) before/after ion adsorption to understand algal surface morphology and the *S. wightii* sorption removal process. The pore radius, diameter, and surface area were determined by the Brunauer-Emmett-Teller Multipoint Analyzer (AutosorbiQ Station 1).

Results and discussion

Effect of pH:

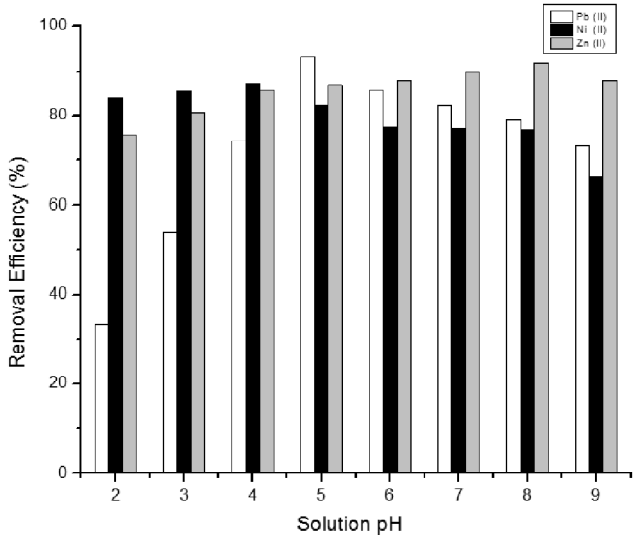

Fig. 1. Influence of equilibrium pH on the metal absorption potential of *S. wightii.*

The pH solution plays an essential role in the measurement of sorbent biosorption. pH is influenced by surface charge, ionization intensity, and functions of surface groups as well as sorption metal ions[21]. Metal removal was first analyzed at equilibrium pH and the results are shown in Fig. 1. With a pH rise from 2 to 9, the percentage of seaweed after elimination of all metal ions became clear with the decrease in pH equilibrium. The reason for this activity was the functional groups of *S. wightii* and speciation of metal ions at different pH levels. The brown algae cell wall primarily consists of polysaccharides including carrageenan and agar. Carboxylate and sulphonate groups are prevalent in numerous functional groups of *S. wightii*. The small pH and negative functional groups are prorogated by H^+ ions and reaction to positive metal ions of Pb^{2+}, Ni^{2+} and Zn^{2+}. As the pH was increased, the number of H^+ ions reduced, and positive metal ions combined with the negatively charged *S. wightii* binding sites[22]. pH greatly affects the speciation of heavy metal ions. Heavy metal ions studied at acidic pH levels (pH ≤ 5) show Pb(II), and Ni(II) as divalent except for Zn(II). Pb(II) and Ni(II) are precipitated at pH values greater than 5 and studies have not been performed above this level for these two metal ions.

Analyzing Fig. 1 shows that *S. wightii* biosorbed Pb^{2+} followed by Zn^{2+} and Ni^{2+}. The attraction to a specific metal ion may be associated with its atomic weight, ion radius, and electron characteristics. The weight of an atom is in the range of Pb (207.2) > Zn (65.4) > Ni (58.7). Conversely, the range for ionic radii, is Pb (119) > Zn (74) > Ni (70) and electronegativity reduced in a range of Pb (2.33) > Ni (1.91) > Zn (1.65). The study consumption of Pb (18.65 mg/g) > Zn (18.40 mg/g) > Ni (17.46 mg/g) was in optimum pH. So a strong association between metal ion biosorption in size and metal properties (atomic weight and ionic radii) was established. Even though Zn electronegativity was less probable relative to the other metals measured, Zn was more biosorbed than Ni due to its atomic weight and ion radii[23].

Characterization studies of S. wightii:

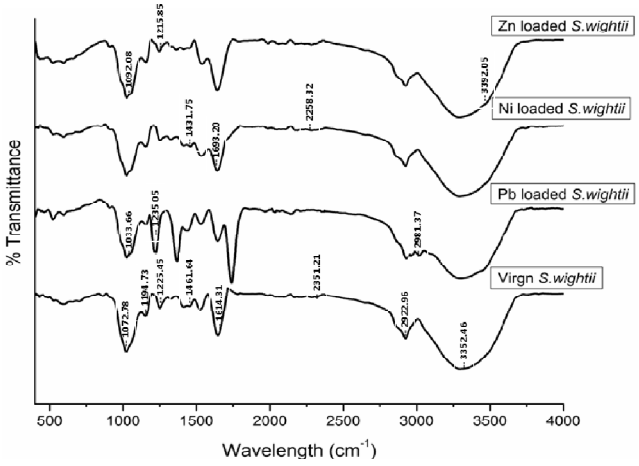

Fig. 2. FTIR spectra of virgin and metal-loaded *S. wightii.*

FTIR spectroscopy analysis of sorption studies was extensively used to detect changes in the frequency rate of

Table 1. Stretching frequencies observed in virgin and metal-loaded *S. wightii*

Functional group	Wavenumber (cm^{-1})			
	Raw *S. wightii*	*S. wightii*-Pb	*S. wightii*-Ni	*S. wightii*-Zn
-OH, -NH stretching	3352.46	3362.16	3352.46	3392.05
Asymmetric CH_2 stretching	2922.96	2981.37	2912.36	2922.96
-P-H- group	2351.21	2287.84	2258.32	2371.50
Asymmetric C=O stretch of COOH	1614.31	1614.31	1693.20	1604.61
Symmetric C=O	1461.64	1451.94	1431.75	1461.64
C-O (COOH) stretching	1225.45	1235.05	1235.05	1215.85
C=C stretching	1194.73	1145.91	1145.91	1135.22
C–O (alcohol) band	1072.78	1033.66	1043.26	1092.08

sorbents and to detect functional groups for the removal of metal ions. In the current analysis, it focused on prior reports that FTIR spectroscopy peaks are attributed to different functional groups. Some chemical classes which include carboxylic, amino, sulfonated, and hydroxyzine were evaluated by seaweed[24]. Fig. 2 illustrates the virgin seaweed FTIR spectra together with *S. wightii* loaded with metal. Virgin *S. wightii* had many absorption levels, demonstrating the dynamic existence of the biosorbent. The seaweed before adsorption displayed peaks at 3352.46 cm^{-1} (-OH, -NH stretching), 2922.96 cm^{-1} (asymmetric CH_2 stretching), 2351.21 cm^{-1} (-P-H- group), 1614.31 cm^{-1} (asymmetric C=O stretch of COOH), 1461.64 cm^{-1} (symmetric C=O), 1225.45 cm^{-1} (C-O (COOH) stretch), 1194.73 cm^{-1} (C=C stretching) and 1072.78 cm^{-1} (C-O (alcohol) band) (Fig. 2). This movement of metal ions in tandem with natural ion species on the biomass surface created adjustments to the wavenumbers detected. Carboxylate biomass was a significant element in metal binding as demonstrated by shifts in peak wavenumbers[25]. Major improvements were specially observed with asymmetric and symmetric C=O and C-O stretches in metal-loaded versus virgin *S. wightii* (Table 1). Additionally, sulphonate group involvement was verified when symmetric and asymmetric-OSO_3 bands were detected with significant changes as opposed to virgin *S. wightii* (Table 1). The findings demonstrated the presence of acidic groups in the bonds of heavy metal ions (carboxyl and sulphonate)[26].

Fig. 3 reveals SEM pictures of virgin and Pb-charged *S. wightii*. The virgin surface of *S. wightii* was composed of sodium and other salt crystalloid deposition protuberances and microstructures. After biosorption, the seaweed's surface was smooth for all metal ions tested in contrast to the virgin state of algae. EDX reports (Fig. 3) were also used to analyze the samples. High Na and K peaks were reported in virgin algae[27] and *S. wightii* acquired these ions from seawater. Fast Pb peaks were observed in the Pb-loaded *S. wightii* sample. In Fig. 3(b), Na peaks disappeared and their frequencies dropped relative to virgin seaweed, indicating that the mechanism of metal exchange was metal removal where light metal ions were exchanged for the captured metal ions during biosorption[28]. The same results were obtained for other metal ions before/after adsorption mechanisms.

Effect of time on metal uptake by S. wightii:

Fig. 4 demonstrates Pb, Ni, and Zn's kinetics of biosorption. *S. wightii*'s biomass allowed the quick t removal of all metal ions under experimental conditions. For all metal ions, *S. wightii* reached 99% complete elimination in 90 min. Following this initial rapid process, a comparatively gradual improvement contributed to a 120-min equilibrium, as seen by a plateau. Therefore, to determine biosorption isotherms, a contact time of 4 h was chosen. The initial rapid period (up to 90 min) may be due to the existence of vacant binding sites during the early stages that can be filled with metal ions. As time passes, repulsive forces between solute molecules during the strong and bulk process render it impossible for the remaining vacant places to be occupied[29,30]. No major variations were found when comparing the concentrations of the three metal ions (Fig. 4). However, adsorption efficiency differed for each metal ion.

The experimental results were based on the pseudo-first

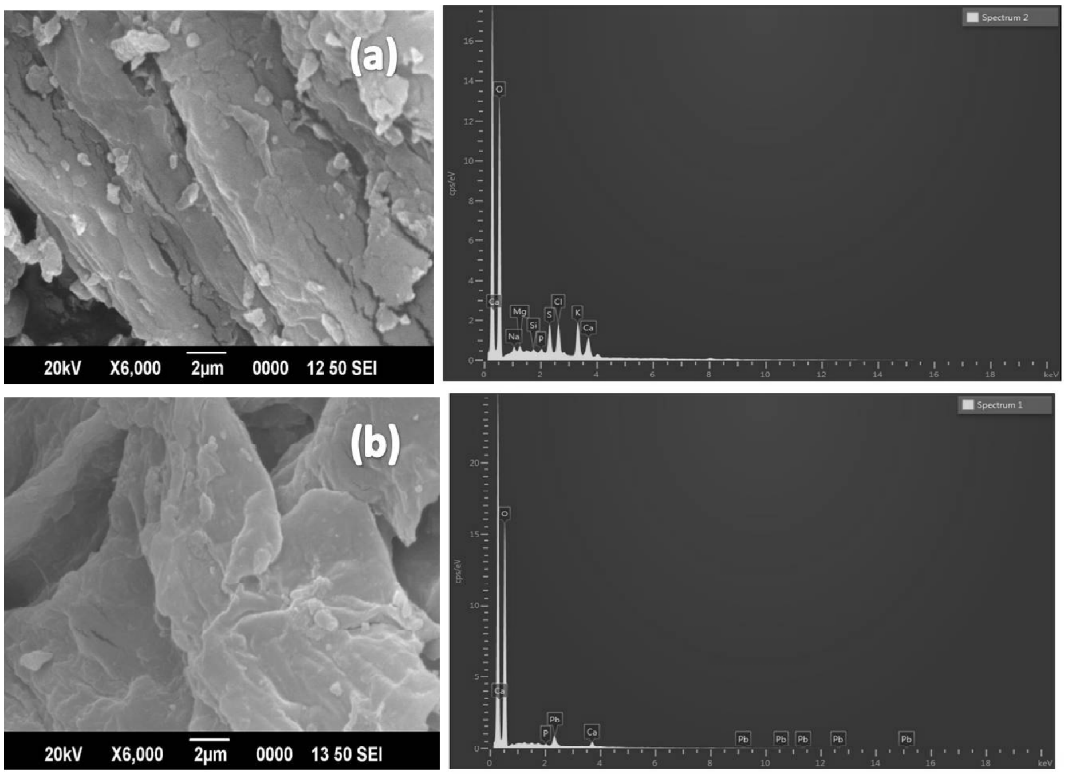

Fig. 3. SEM and EDX images of (a) virgin and (b) Pb-loaded *S. wightii.*

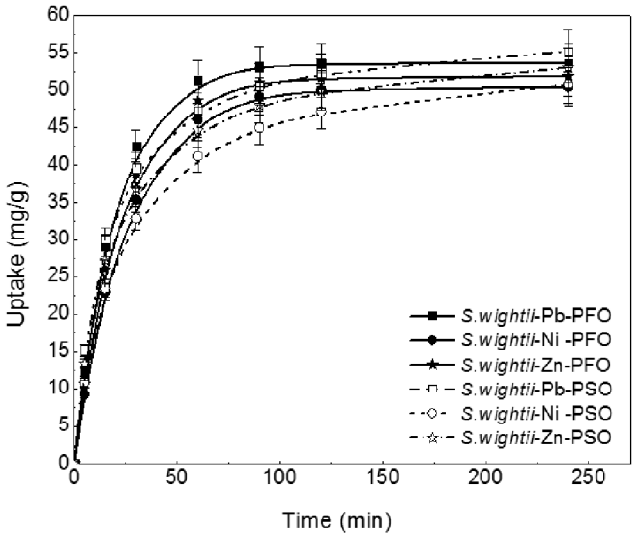

Fig. 4. Kinetics of *S. wightii* toward Pb(II), Ni(II) and Zn(II) metal ions concentration of 100 mg/L.

and second-order models to approximate the kinetics of metal absorption and variations in biosorption kinetic speeds. The models are listed below,

$$\text{Pseudo-first order model: } Q_t = Q_e\,(1 - \exp(-k_1 t)) \qquad (2)$$

$$\text{Pseudo-second order model: } Q_t = \frac{Q_e^2 k_2 t}{1 + Q_e k_2 t} \qquad (3)$$

Q_t is the sorption capacity at any time t (mg/g), Q_e is the sorption capacity in equilibrium time (mg/g), and k_1 the constant of pseudo-first order (min^{-1})[31,32]. Table 2 introduces the model constants along with the correlation coefficient (R^2) values. Throughout pseudo-first order simulations, experimental kinetics with very high R^2 values were shown (Table 2). The value of Q_e was expected in the following order: Pb > Zn > Ni. Q_e values from the experiment were 53.143, 51.021, and 49.128 mg/g, for Pb, Zn, and Ni as predicated, respectively. It is because of a time lag, likely due to a boundary layer or external resistance regulating the initial step of the sorption cycle that resulted in variations in the forecast[33]. In comparison, Q_e values were over predicted in the experiment for second order kinetics (Table 2). Several reports showed that the Pseudo model appears to overestimate Q_e

Table 2. Isotherm and kinetic model constants obtained during metal biosorption in *S. wightii*

Models	Constants	*S. wightii*-Pb	*S. wightii*-Ni	*S. wightii*-Zn
Langmuir	Q_{max}	89.900	57.034	68.335
	b_L	0.203	0.122	0.168
	R^2	0.932	0.955	0.952
Freundlich	K_F	12.351	9.219	11.147
	n_f	0.658	0.543	0.613
	R^2	0.891	0.971	0.977
Sips	K_S	25.554	16.250	19.696
	β_S	0.739	0.640	0.719
	a_S	0.644	0.607	0.632
	R^2	0.994	0.998	0.996
Toth	Q_{max}	86.367	56.740	70.156
	b_T	0.224	0.110	0.158
	n_T	2.316	1.920	1.948
	R^2	0.997	0.999	0.998
Pseudo-first order	Q_e	53.143	49.128	51.021
	k_1	0.0526	0.0405	0.0463
	R^2	0.998	0.994	0.996
Pseudo-second order	Q_e	58.488	55.032	56.536
	k_2	0.0012	0.0009	0.0011
	R^2	0.991	0.992	0.991

values. Fig. 4 shows kinetics curves in comparison with the experimental kinetic data with pseudo-first and second-order models. A Conceptual illustration of heavy metal sorption mechanisms on the surface of the biosorbent is given in Fig. 5.

Biosorption isotherms:

Fig. 6 shows the Pb, Ni, and Zn equilibrium biosorption by *S. wightii*. To evaluate the maximum saturation capability of any sorbent, sorption isotherms are critical and are the plot in the solution for the sorption uptake (Q) vs the equilib-

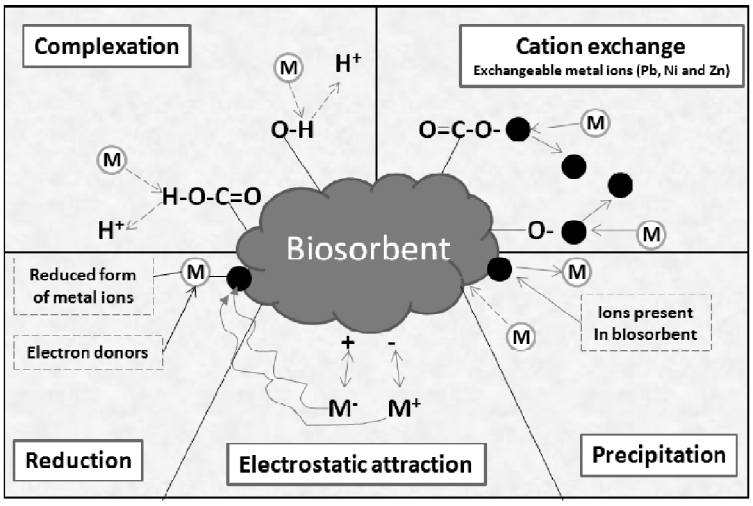

Fig. 5. Conceptual illustration of heavy metal sorption mechanisms on the surface of the biosorbent.

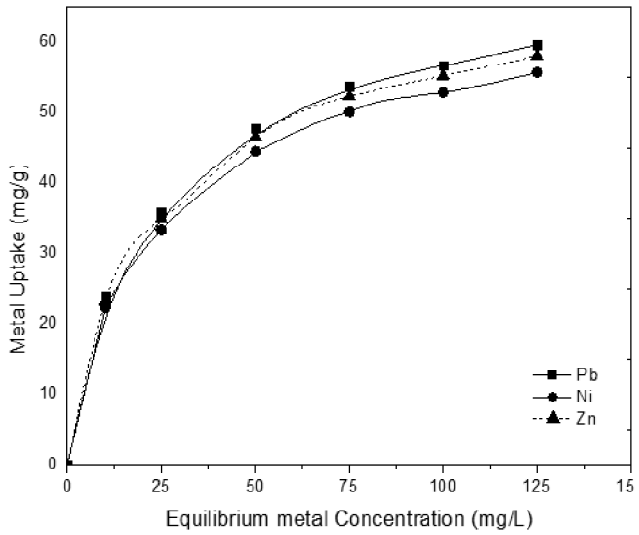

Fig. 6. Toth model isotherms of different metal ions.

rium metal level (C_e). Different initial metal concentrations in a range of 10–125 mg/L were established in this analysis to achieve optimum pH biosorption isotherms, which typically rise dramatically during the initial phases, hitting the slightly curved lines with greater initial metal concentrations. The sharp rise in the initial phases is attributed to the moles of metal ions, of readily accessible sites in the adsorbent. Improvement in the concentration of metal ions reduces the ratio of the binding positions to metal ions moles[34]. Fig. 6, reveals that all three metal ions provided a desirable slight curved isotherm. It was obvious that the isotherm obtained by Pb showed a steep slope accompanied by Zn and Ni. In comparison, Pb (59.44 mg/g) > Zn (58.54 mg/g) > Ni (56.64 mg/g) were in the experimental uptake order.

Two and three-parameter models were used to compare the experimental isotherms as follows,

$$\text{Freundlich model: } Q = K_F C_e^{1/n_F} \quad (4)$$

$$\text{Langmuir model: } Q = \frac{Q_{max} b_L C_e}{1 + b_L C_e} \quad (5)$$

$$\text{Toth model: } Q = \frac{Q_{max} b_T C_e}{[1 + (b_T C_e)^{1/n_T}]^{n_T}} \quad (6)$$

$$\text{Sips model: } Q_e = \frac{K_S C_e^{\beta_s}}{1 + a_S C_e^{\beta_s}} \quad (7)$$

where Q_{max} is maximum sorption capacity (mg/g), b_L is a constant of Langmuir (L/mg), K_F a constant of Freundlich (mg/g) $(L/mg)^{1/n_F}$, n_F an exponent of Freundlich, K_S a constant of Sips (L/g), a_S the coefficient of Sips (L/mg), β_S an exponent of Sips; b_T a constant of Toth (L/mg) and n_T an exponent of Toth. These models were selected for their simple consistency and easy constants.

Table 2 displays the model constants. Originally, the Langmuir model represented the experimental isotherm results. This model was able, with high correlation values (R^2 > 0.932), to characterize the isotherm results. Originally for gas absorption, the Langmuir concept was widely used for biosorption. According to the model, that position preserves one molecule and all sites are not dependent on the energy of the adsorbed quantity. Moreover, the Langmuir model estimates the optimum potential of biosorption in any biomass that cannot be reached during experiments[35]. *S. wightii* displayed a strong Pb Q_{max} value, accompanied by Zn and Ni as shown in Table 2. In other terms, metal ion attraction to the sorbent decreased with metal ion size. The Freundlich model data was considerably lower than that of the Langmuir model (Table 2). As the Freundlich isotherm is linear, only small to moderate concentration levels can be fairly applied. The concept was originally empirical, but, heterogeneous surfaces or surface sites that support numerous affinities have subsequently been interpreted[36]. Both the Freundlich isotherm constant (K_F) and exponent (n_F) were reported high for Pb, Zn, and Ni (Table 2) respectively.

For this analysis, three-parameter models were used to improve the studies further. The Sips model, a combined method for isotherm equations was developed by Freundlich and Langmuir to simulate heterogeneous adsorption processes. At low concentrations of solvents, the model decreases to Freundlich and forecasts the Langmuir formula at high concentrations[37]. A successful prediction was obtained with the use of the Sips variant of the experimental data (R^2 > 0.994). The Sips isotherm constant (K_S) model reported high for Pb with three metal ions, followed by Zn and Ni. The Sips function exponent (β_S), which implies that the isotherm details are more of the Langmuir type than the Freundlich type is similar to unity (Table 2). The Toth model suggests an asymmetrical quasi-Gaussian, energy distribution, while most places are lower than their limit or the mean energy adsorption[38]. Compared to other factors it was strong for Pb,

followed by Zn and Ni, in a magnitude of the Toth model isothermic constant. The Toth model defined the isotherm metal biosorption data better, based on $R^2 > 0.997$, and explains the expected curves in Fig. 6.

Desorption studies:

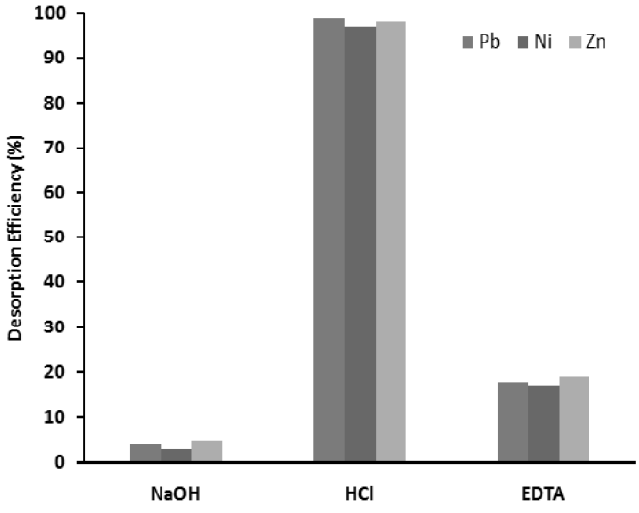

Fig. 7. Desorption of different elutants for metal-loaded *S. wightii.*

The reuse of biomass is important for any efficient biosorption operation, as it decreases both the method's cost and the process of continuous sorbent supply. The appropriate choice of eluting agents based on biosorbent type and biosorption mechanism is important to ensure a good desorption process[39,40]. Seeing that *S. wightii* biosorption and the maximal biosorption occurred under moderate acid conditions, an ion exchange process (Fig. 1) was investigated with the three elutants, 0.01 *M* HCl, NaOH, and EDTA. Tests also showed that *S. wightii* metal ions cannot be extracted from 0.01 *M* NaOH and EDTA solutions, while efficiencies of low elution were observed for all metal ions (Fig. 7). Conversely, a strong elution output was induced by exposure of metal loaded *S. wightii* to 0.01 *M* HCl. This high efficiency facilitated the postulated ion exchange for biosorption, as desorbent H^+ ions are shared with attached metal ions in a negative loaded functional group. It ensures that 0.01 *M* HCl can be used successfully in biosorption for the regeneration of *S. wightii*. EDTA is considered a strong complexing agent with 6 active coordinates sites that contain -COOH and $-NH_2$ and mostly form 1:1 complex with many metal ions. The solution's pH plays a major role between the metal ion to be desorbed and the chelating agent is EDTA. EDTA has maximum desorption efficiency mostly at neutral pH but losses its chelating effect in acidic and base conditions. This may result in less desorption efficiency.

Conclusion

The following conclusions were arrived at from the current study,

(a) We studied brown seaweed *Sargassum wightii* as an important sorbent for the removal of Pb(II), Ni(II) and Zn(II) ions.

(b) Results from experiments showed that *S. wightii*'s biosorption ability with pH 5, 4, and 8 for Pb, Ni, and Zn were highly influenced by pH for maximal ions elimination.

(c) SEM and FTIR analysis was used to understand the removal process mechanism. Toth isotherm model data revealed that *S. wightii* had a higher adsorption capacity of Pb (86.37 mg/g), accompanied by Zn (70.16 mg/g) and Ni (56.74 mg/g).

(d) Biosorption kinetics for all metal ions was observed rapidly with equilibrium within 90 min.

(e) Elution efficiency greater than 97% desorbed metal ions in *S.wightii* were successful with 0.01 *M* HCl. This seaweed-based treatment is an attractive and viable technique to extract Pb(II), Ni(II), and Zn(II) from wastewater with easy access, high biosorption efficiency, fast removal, and quick desorption.

References

1. F. F. Çeçen, *Hazardous Pollutants in Biological Treatment Systems*, 2018, 123.
2. W. Xu and M. Duran, 2018, 239.
3. D. Maiti, I. Ansari, M. A. Rather and A. Deepa, *Water Sci. Technol.*, 2019, **79**, 2023.
4. J. Jegan, J. Vijayaraghavan, T. Bhagavathi Pushpa and S. J. Sardhar Basha, *Desalin. Water Treat.*, 2016, **57**, 25812.
5. J. Thivya and J. Vijayaraghavan, *Desalin. Water Treat.*, 2019, **167**, 333.
6. J. Kanagaraj, T. Senthilvelan, R. C. Panda and S. Kavitha, *J. Cleaner Prod.*, 2015, **89**, 1.
7. H. Li, X. Dong, E. B. da Silva, L. M. de Oliveira, Y. Chen and L. Q. Ma, *Chemosphere*, 2017, **178**, 466.
8. S. Kiran, A. Adeel, S. Kamal, M. Saeed, F. U. Rehman and T. Gulzar, "Handbook of Textile Effluent Remediation", Pan Stanford Publishing Pvt. Ltd., Singapore, 2018.

9. N. Tamilselvan, K. Saurav and K. Kannabiran, *J. Ocean Univ. China*, 2011, **11**, 52.
10. R. Senthilkumar, D. M. R. Prasad, L. Govindarajan, K. Saravanakumar and B. S. N. Prasad, *Environ. Technol*., 2017, **40**, 1262.
11. L. P. Mazur, M. A. P. Cechinel, S. M. A. G. U. de Souza, R. A. R. Boaventura and V. J. P. Vilar, *J. Environ. Manage*., 2018, **223**, 215.
12. S. B. Nasab, A. Homaei and L. Karami, *Biocatal. Agric. Biotechnol*., 2020, **23**, 101478.
13. M. Prodromou and I. Pashalidis, *Desalin. Water Treat*., 2015, **57**, 5079.
14. J. Marimuthu, @Antonisamy, P. Essakimuthu, J. Narayanan, B. Anantham, R. J. J. M. Tharmaraj and S. Arumugam, *Asian Pac. J. Trop. Dis*., 2012, **2**, 109.
15. R. S. Praveen and K. Vijayaraghavan, *Desalin. Water Treat.*, 2014, **55**, 1816.
16. M. A. Hashim and K. H. Chu, *Chem. Eng. J*., 2004, **97**, 249.
17. K. Vijayaraghavan, J. Jegan, K. Palanivelu and M. Velan, *Sep. Purif. Technol*., 2005, **44**, 53.
18. A. A. Prabhu, S. Chityala, D. Jayachandran, N. N. Deshavath and V. D. Veeranki, *Sep. Sci. Technol*., 2020, 1.
19. S. Rangabhashiyam, M. S. GiriNandagopal, E. Nakkeeran, R. Keerthi and N. Selvaraju, *Desalin. Water Treat.*, 2016, **57**, 26101.
20. S. Rangabhashiyam, E. Suganya, N. Selvaraju and L. A. Varghese, *World J. Microbiol. Biotechnol.*, 2014, **30**, 1669.
21. A. Verma, S. Kumar and C. Balomajumder, *Desalin. Water Treat*., 2019, **170**, 239.
22. M. Tukarambai and P. Venakateswarlu, Mater. Today: Proc., 2019.
23. M. Torab-Mostaedi, M. Asadollahzadeh, A. Hemmati and A. Khosravi, *Res. Chem. Intermed.*, 2013, **41**, 559.
24. R. Gokulan, A. Avinash, G. G. Prabhu and J. Jegan, *J. Environ. Chem. Eng.*, 2019, **7**, 103297.
25. N. K. Gupta, A. Sengupta, A. Gupta, J. R. Sonawane and H. Sahoo, *J. Environ. Chem. Eng*., 2018, **6**, 2159.
26. J. Vijayaraghavan, T. Bhagavathi Pushpa, S. J. Sardhar Basha, K. Vijayaraghavan and J. Jegan, *Sep. Sci. Technol*., 2014, **50**, 1120.
27. R. Gokulan, G. Ganesh Prabhu and J. Jegan, *Water Environ. Res.*, 2019, **91**, 642.
28. K. Vijayaraghavan and T. Ashokkumar, *J. Environ. Chem. Eng*., 2017, **5**, 4866.
29. K. Vijayaraghavan and J. Jegan, *J. Rare Earths*, 2015, **33**, 1196.
30. S. Deng, P. Wang, G. Zhang and Y. Dou, *J. Hazard. Mater.*, 2016, **307**, 64.
31. T. Bhagavathi Pushpa, J. Vijayaraghavan, S. J. Sardhar Basha, V. Sekaran, K. Vijayaraghavan and J. Jegan, *Ecotoxicol. Environ. Saf.*, 2015, **118**, 177.
32. J. Thivya and J. Vijayaraghavan, *Desalin. Water Treat*., 2019, **156**, 87.
33. S. Deng, G. Zhang, S. Chen, Y. Xue, Z. Du and P. Wang, *J. Mater. Chem. A*, 2016, **4**, 15851.
34. C. M. Coelho, J. R. de Andrade, M. G. C. da Silva and M. G. A. Vieira, *Environ. Sci. Pollut. Res*., 2020.
35. Y. Chen, B. Wang, J. Xin, P. Sun and D. Wu, *Ecotoxicol. Environ. Saf*., 2018, **164**, 440.
36. K. Vijayaraghavan, U. M. Joshi and S. Kamala-Kannan, *Ecological Engineering*, 2012, **47**, 278.
37. K. Vijayaraghavan, S. Rangabhashiyam, T. Ashokkumar and J. Arockiaraj, *J. Taiwan Inst. Chem. Eng.*, 2017, **74**, 113.
38. T. Bhagavathi Pushpa, J. Vijayaraghavan, K. Vijayaraghavan and J. Jegan, *Desalin. Water Treat*., 2016, **57**, 24368.
39. M. J. Ahmed, P. U. Okoye, E. H. Hummadi and B. H. Hameed, *Bioresour. Technol*., 2019, **278**, 159.
40. G. Zeng, C. Hong, Y. Zhang, H. You, W. Shi, M. Du and B. Chen, *Water, Air, Soil Pollut*., 2020, **231**.